Science Advances

AAAS

advances.sciencemag.org/cgi/content/full/2/11/e1600445/DC1

Supplementary Materials for

Glacial to Holocene changes in trans-Atlantic Saharan dust transport and dust-climate feedbacks

Ross H. Williams, David McGee, Christopher W. Kinsley, David A. Ridley, Shineng Hu, Alexey Fedorov, Irit Tal, Richard W. Murray, Peter B. deMenocal

Published 23 November 2016, *Sci. Adv.* **2**, e1600445 (2016)
DOI: 10.1126/sciadv.1600445

The PDF file includes:

Other Supplementary Material for this manuscript includes the following:
(available at advances.sciencemag.org/cgi/content/full/2/11/e1600445/DC1)

- data file S1 (Microsoft Excel format). U-Th data and dust fluxes.
- data file S2 (Microsoft Excel format). Radiocarbon data from core VM20-234.
- data file S3 (Microsoft Excel format). Trace element data from Bahamas sediments.

Supplementary Materials and Methods

1. Site descriptions and age models

1.1 Bahamas sites OCE205-2 100GGC and 103GGC

Cores 100GGC and 103GGC were taken within the Northwest Providence Channel between the Great Bahama Bank and the Little Bahama Bank (fig. S1) during the 1988 cruise OCE 205-2 of the R/V Oceanus. Both cores were obtained with a giant gravity corer. The channel consists of a large canyon with many small canyons extending from it. During the Holocene, the region has remained stable with little downslope slumping of shelf material (*78*). Modern and Holocene sedimentation in the channel is dominated by carbonate precipitated on the bank tops and exported to deeper waters (*79*), with terrigenous material dominantly coming from an eolian source (*11*, *36*). Water transport into the NW Providence Channel is primarily from the open-ocean Atlantic (Sargasso Sea) (*80*), and sediment composition shows no evidence of sedimentary inputs from the Florida Strait (*28*).

Age control is provided by 15 radiocarbon ages in 103GGC and 13 in 100GGC. Radiocarbon measurements were conducted on monospecific samples of planktonic foraminifera (*G. sacculifer* or *G. ruber*), with one sample consisting of a mixture of the two species (*81*, *82*). Radiocarbon ages were calibrated using Marine13 (*83*) and a constant reservoir age of 400 years. Ages for each depth were calculated using median ages from the P Sequence routine within Oxcal (*84*) (fig. S2).

As is typical for channel and slope sites in the Bahamas (*85*), sedimentation rates are low during the last glacial period and deglaciation (2 cm/ka) and increase after 13 ka to 8-10 cm/ka. The increase in sedimentation rates is accompanied by a change in the focusing factor, the ^{230}Th-derived estimate of the ratio of total sediment accumulation to sediment inputs from the overlying water column. The focusing factor is calculated as the ratio of xs^{230}Th inventory within a dated interval of the sediment divided by the xs^{230}Th production rate in the overlying water column during the same period of time (*43*); a focusing factor of 1 implies no lateral inputs or removal of sediment. From 13-20 ka, the focusing factor in 103GGC is 1.7, implying relatively limited focusing. After 13 ka, the focusing factor averages 4.8,

consistent with increased supply of aragonite from banktops. There is no systematic difference in focusing factors between the early and late Holocene (fig. S3).

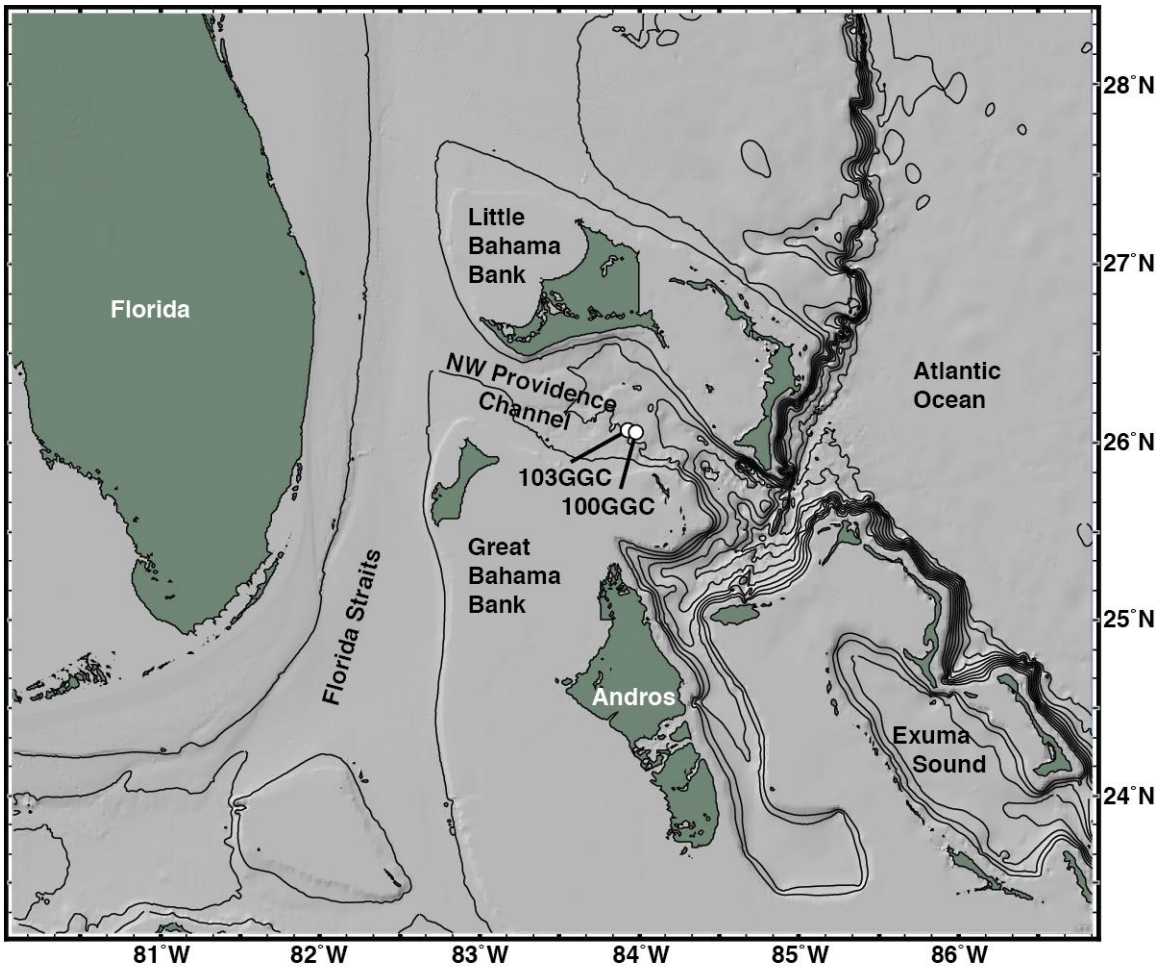

fig. S1. Map showing core sites for Bahamas cores OCE205-2 100GGC and 103GGC. Contour interval is 500 m. Map was made using GeoMapApp (geomapapp.org).

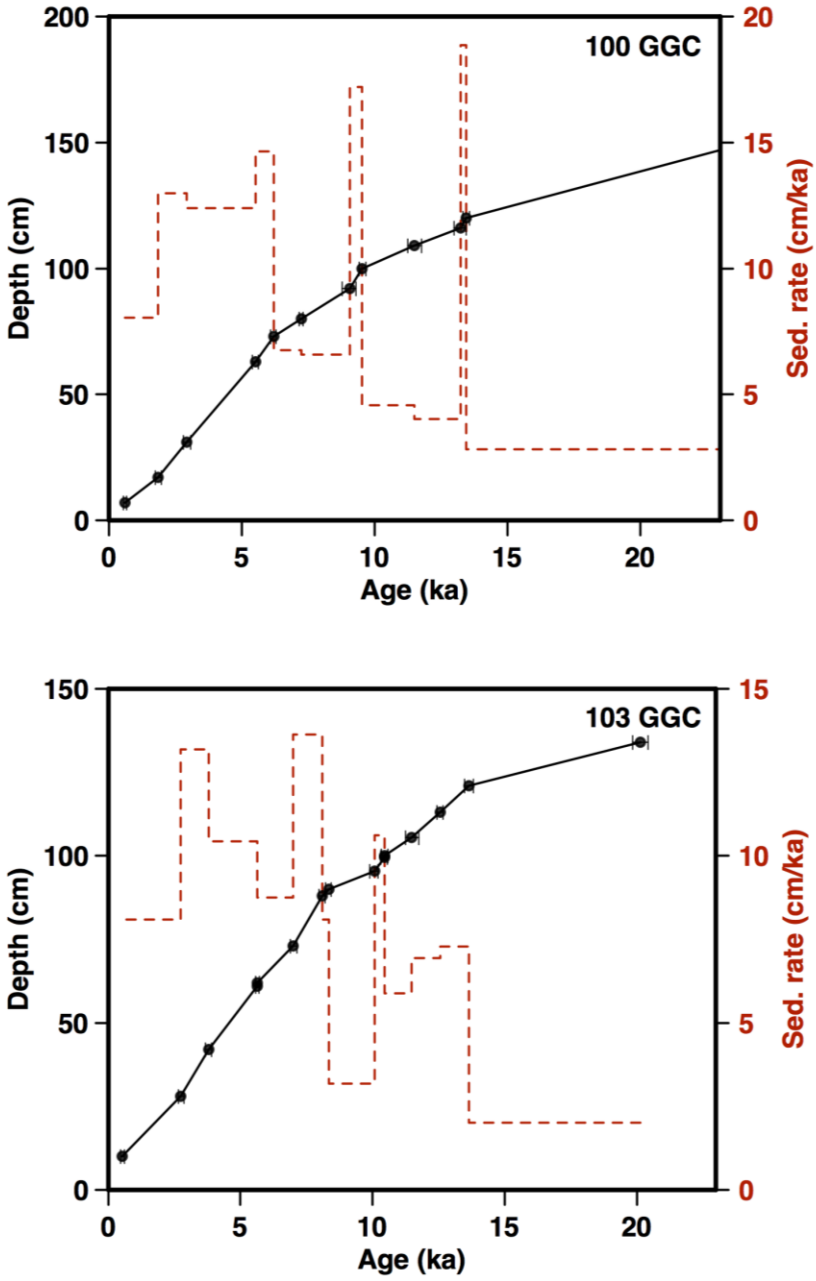

fig. S2. Age-depth plots for OCE205-2 100GGC and 103GGC. Vertical axis is in units of cm from the top of the core. Note the substantial increase in sedimentation rates in sediments younger than ~13 ka. 95% confidence intervals on calibrated ^{14}C ages are shown.

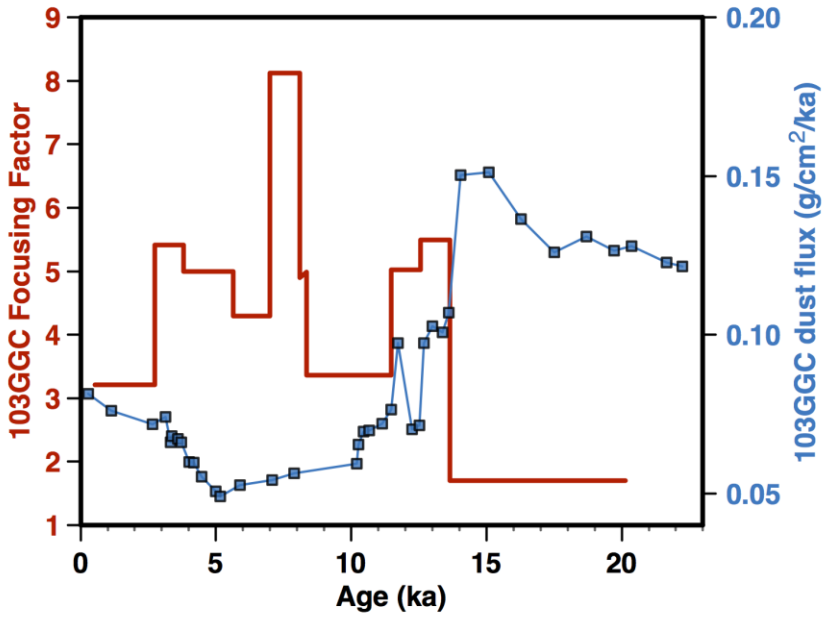

fig. S3. Comparison of focusing factors and reconstructed dust fluxes in core 103GGC. Note that there is no discernable relationship between focusing factors (red) and dust fluxes (blue) over the last 13 ka despite factor of 2.5 changes in focusing factor, suggesting that variable additions of banktop sediments do not significantly impact the Holocene changes reconstructed in this study, and that the change in focusing factor at ~13 ka is unlikely to explain the majority of the flux difference between the deglacial and Holocene portions of the core.

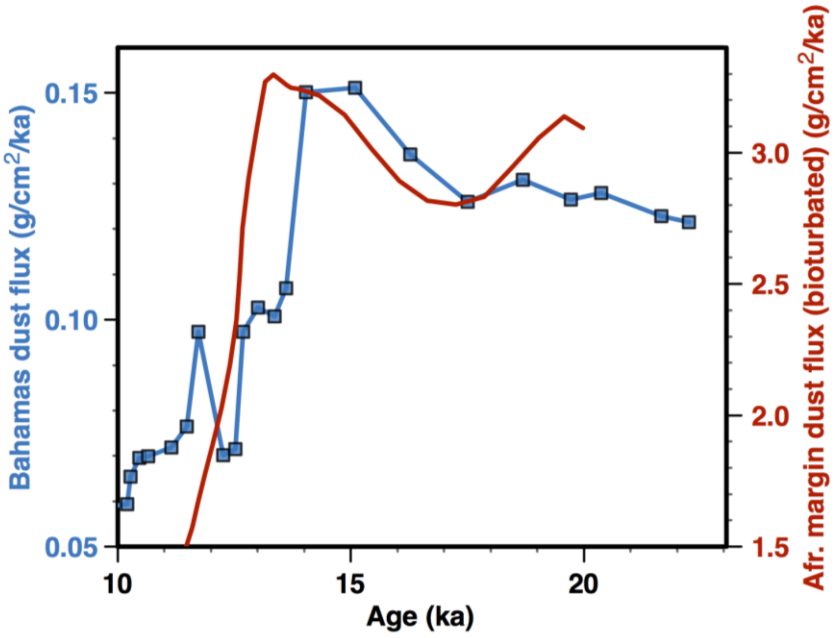

fig. S4. Test of the impact of bioturbation on the deglacial portion of the Bahamas record. The deglacial Bahamas record from core 103GGC (blue) is compared with the GC68 African margin record smoothed with a simple bioturbation model (red). The similarity of the bioturbated African margin record and the observed deglacial Bahamas record suggests that dust fluxes in the Bahamas also peaked during the Heinrich 1 and Younger Dryas stadials. The original GC68 record is shown in Fig. 2.

1.2 Tropical Atlantic site VM20-234

Sediment core VM20-234 was taken along the Mid-Atlantic Ridge at 5.317˚N, 33.033˚W and a water depth of 3133 m (fig. S5). The core was retrieved using a piston coring device by the R/V Vema in 1964 and is primarily composed of a foraminiferal chalk ooze with common manganese oxides.

Age control is provided by 8 radiocarbon ages plus 2 replicates on samples of planktonic foraminifera (*G. sacculifer* and/or *G. ruber*) (table S2; fig. S6). Six samples were analyzed at the Center for Accelerator Mass Spectrometry at Lawrence Livermore National Laboratory, and four were analyzed at the National Ocean Sciences Accelerator Mass Spectrometry facility at Woods Hole Oceanographic Institution. Radiocarbon ages were calibrated using Marine13 (*83*) and a constant reservoir age of 400 years. Age models were determined using the P Sequence routine within Oxcal (*84*). Two ages (at 1.5 and 66 cm) were not included in the age model, as their inclusion would require two intervals of nearly instantaneous deposition of 10-30 cm of sediment at this open-ocean site. The inclusion of these ages in the age model alters the shape of the deglacial fall in dust flux but does not change the Holocene record significantly.

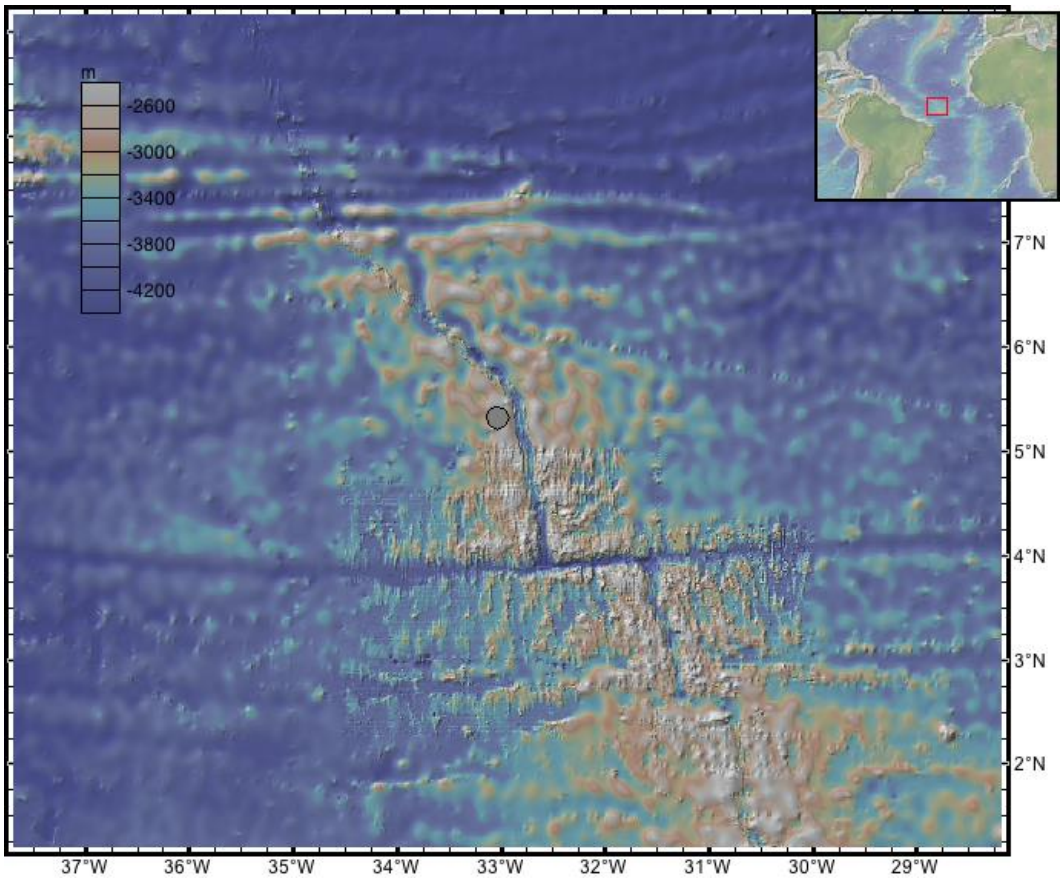

fig. S5. Map showing core site for core VM20-234 along the Mid-Atlantic Ridge. Map was made using GeoMapApp (geomapapp.org).

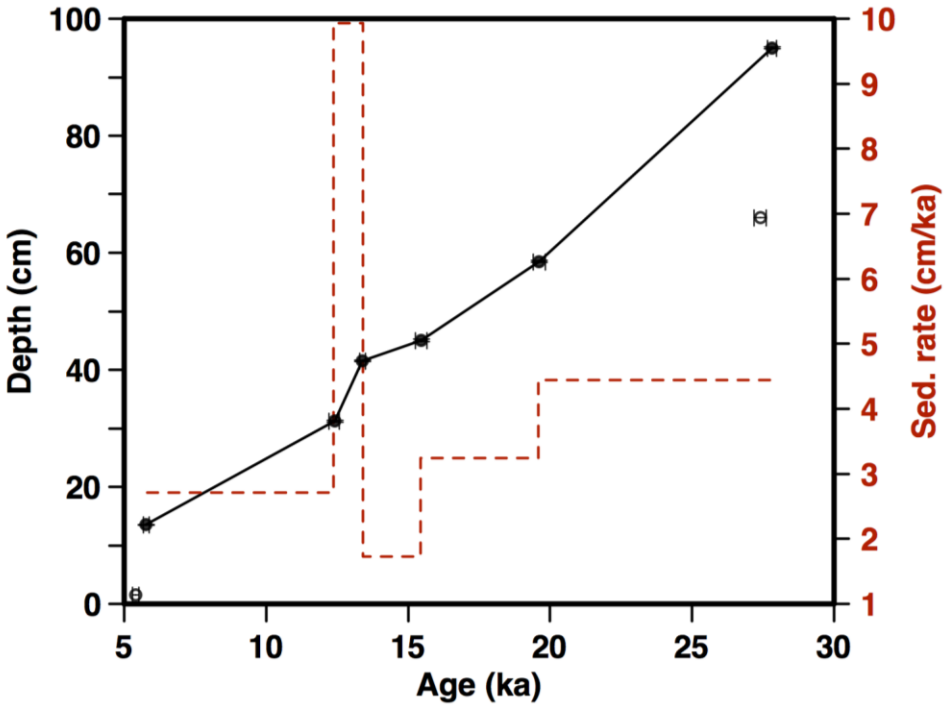

fig. S6. Age-depth plot and sedimentation rates for VM20-234. Two excluded ages are indicated by open circles. 95% confidence intervals on calibrated ^{14}C ages are shown.

2. Dust flux measurements and uncertainties

2.1 U-Th measurements

Samples weighing 40-100 mg were combined with ^{229}Th and ^{236}U spike solutions in PFA beakers. Following dissolution of carbonates in 8 N nitric acid, samples were digested in a combination of nitric, hydrofluoric and perchloric acids in a closed-system digestion block (Analab Evapoclean) and then dried down. Samples were re-dissolved in 1 N hydrochloric acid and transferred to 15 mL centrifuge tubes. Soluble ions (e.g., Ca) were then separated from U and Th by iron oxy-hydroxide precipitation. Dissolved Fe was added to the Bahamas samples for this step, while no Fe had to be added to the Mid-Atlantic Ridge samples. Ammonium hydroxide was added to precipitate iron oxy-hydroxides and scavenge uranium and thorium, followed by centrifugation and two water rinses to decant the supernatant containing soluble ions. Iron oxides were dissolved in 8 N nitric acid, and U and Th were purified by passing through 2 mL columns packed with AG1-X8 resin (BioRad). Separate U and Th fractions were dried down and taken up in 1 mL of 0.3 M nitric acid.

Samples from the Bahamas cores were analyzed using a Thermo Scientific Neptune Plus multi-collector ICP-MS at Brown University, and samples from VM20-234 were analyzed using a Nu Plasma II-ES multi-collector ICP-MS at MIT. ^{230}Th and ^{234}U were analyzed on a secondary electron multiplier and all other isotopes were simultaneously measured on Faraday cups. A uranium standard (CRM 112a) and an internally calibrated thorium standard (^{229}Th-^{230}Th-^{232}Th) were used to track mass bias and SEM yield for U and Th fractions, respectively. Half mass measurements were conducted on all Th samples to estimate tailing of ^{232}Th on ^{230}Th. Uncertainties on isotope ratios after correction for tailing, mass bias, SEM yield, and background were always <1%. Procedural blanks were processed with each set of samples and were always <1%. Aliquots of an internal sediment standard were processed with each set of 8-18 samples to monitor reproducibility. The relative standard deviation of ^{232}Th/^{230}Th ratios for 11 separately processed aliquots of this standard analyzed over the course of the study is 0.8%.

2.2 Dust flux estimate uncertainties

Uncertainties in ^{230}Th-normalized fluxes derived from analytical uncertainty and corrections for supported ^{230}Th are 3% or less for all samples. Larger and less easily quantified are uncertainties related to the assumptions that 1) ^{230}Th fluxes in descending particles are equal to the ^{230}Th production rate in the overlying water column; 2) descending particles and sediments transported downslope have similar ^{230}Th concentrations; and 3) ^{232}Th concentrations in dust deposited at the sites are estimated accurately. We consider each of these sources of uncertainty in the paragraphs that follow.

Modeling and sediment trap studies suggest that the first assumption is correct to within 30% in most sedimentary environments (*44*, *86*, *87*), with departures of only ~40% even in regions with extreme gradients in Th scavenging (*88*). Moreover, offsets between water column production and the vertical rain of ^{230}Th are likely to remain relatively constant downcore if sedimentation regimes remain similar through time (*89*), making the uncertainty in relative changes in accumulation rates substantially smaller than 30%. This argument applies to comparisons of flux changes within the Holocene portion of the cores – the main focus of this study – and to comparisons within the LGM/deglacial portion of the cores, but may not apply to comparisons between the two sections in the Bahamas due to the substantial change in focusing and sediment composition between the two portions of the core. This point is considered in more detail below. Deglacial changes in sedimentary composition are smaller but still significant at VM20-234, as the >63 μm fraction (a proxy for carbonate percentage) averages 20% during the LGM and 35% in the Holocene with no difference between the early and late Holocene.

At VM20-234, the main concern with employing $^{230}Th_{xs}$ normalization is that iron and manganese oxides precipitating from the hydrothermal plume at the Mid-Atlantic Ridge scavenge dissolved Th. Scavenging of dissolved Th in the hydrothermal plume at the TAG site along the Mid-Atlantic Ridge at 26˚N reduces bottom water ^{230}Th concentrations by a factor of ~3-6 (*88*). This reduction could cause anomalous dissolved ^{230}Th supply to the water column above the core site by transport down concentration gradients, leading to an underestimation of sediment fluxes.

We can estimate the quantitative importance of this effect in multiple ways. First, anomalous dissolved ^{230}Th supply and burial at the VM20-234 core site should result in an unusually high ^{230}Th-based

focusing factor. The average focusing factor over the last 21 ka is only 1.7-2.4 (assuming sedimentary dry bulk density of 0.5-0.7, typical for carbonate-rich deep-sea sediments (*90*)), fairly typical for sites selected for sediment coring, especially given widespread seismic evidence for sediment ponding near the complex topography of the Mid-Atlantic Ridge (*91*). Second, we can compare our coretop sediment flux estimates to estimates of modern dust deposition in the region. As shown in the main text, there is very good agreement. Third, the magnitude of the terrigenous fluxes reconstructed at VM20-234 is very close to ^{230}Th-normalized terrigenous fluxes measured at 3 sites at 4-5˚N, 20-21˚W on the Sierra Leone Rise (*49*), which is not near the Mid-Atlantic Ridge: 0.28 g/cm^2/ka at the Mid-Atlantic Ridge vs. ~0.35 g/cm^2/ka at the Sierra Leone Rise in the Late Holocene, and 0.7 g/cm^2/ka at the Mid-Atlantic Ridge vs. ~0.6 g/cm^2/ka at the Sierra Leone Rise at the LGM. This good agreement despite the lack of hydrothermal inputs at the Sierra Leone Rise suggests that hydrothermal impacts on VM20-234 fluxes are small.

The second assumption, that descending particles and sediments transported downslope have similar ^{230}Th concentrations, is pertinent in the Bahamas, where offshore transport of resuspended shallow-water carbonates has been the dominant source of sediment to the core sites during the Holocene. The accuracy of ^{230}Th$_{xs}$ normalization in this regime is supported by studies in other continental margin environments, which show good reproducibility of fine-fraction fluxes in cores with quite different rates of downslope sediment addition (*92–94*).

Even so, the large difference in focusing factor before and after 13 ka (1.7 from 13-20 ka vs. 4.8 after 13 ka) may cause an offset in ^{230}Th-normalized accumulation rates between the deglacial and Holocene portions of the Bahamas cores if lateral additions alter the ^{230}Th concentrations or ^{232}Th/^{230}Th ratios in the core. (For definition of focusing factor, see Supplementary Information Section 1.1.) Examples of processes that could cause such a focusing-related offset are a) incomplete equilibration of advected sediments with water column ^{230}Th prior to burial and b) fractionation of windblown dust from fine aragonitic sediments during lateral transport.

We can estimate the potential magnitude of focusing-related offsets by examining the relationship between focusing factor and dust flux during the Holocene in core 103GGC (fig. S3). We note no consistent relationship between focusing factor and dust flux over the last 13 ka, suggesting that

focusing changes of a factor of 2 have limited impact on reconstructed dust fluxes. This observation, in combination with previous work in margin settings (*92–94*), suggests that any offset in the absolute magnitude of dust flux between the deglacial and Holocene portions of the core is likely to be much smaller than the factor-of-two difference between peak deglacial fluxes and coretop fluxes.

The third assumption, that ^{232}Th concentrations in dust deposited at the core sites can be estimated accurately based on measurements of fine-grained African dust at Barbados (*11*), is reasonable given the consistency of ^{232}Th concentrations in global dust sources (*45*).

Uncertainties shown in Fig. 2 and in table S1 reflect analytical uncertainties, uncertainties in the calculation of $^{230}Th_{xs}$ from total ^{230}Th, and uncertainties in the ^{232}Th concentration of African dust. We do not include uncertainties related to the accuracy of $^{230}Th_{xs}$ normalization at these core sites; as stated above, these uncertainties in absolute fluxes are likely on the order of 30%, but are substantially smaller for comparisons of relative changes downcore at the same site, the main focus of this paper.

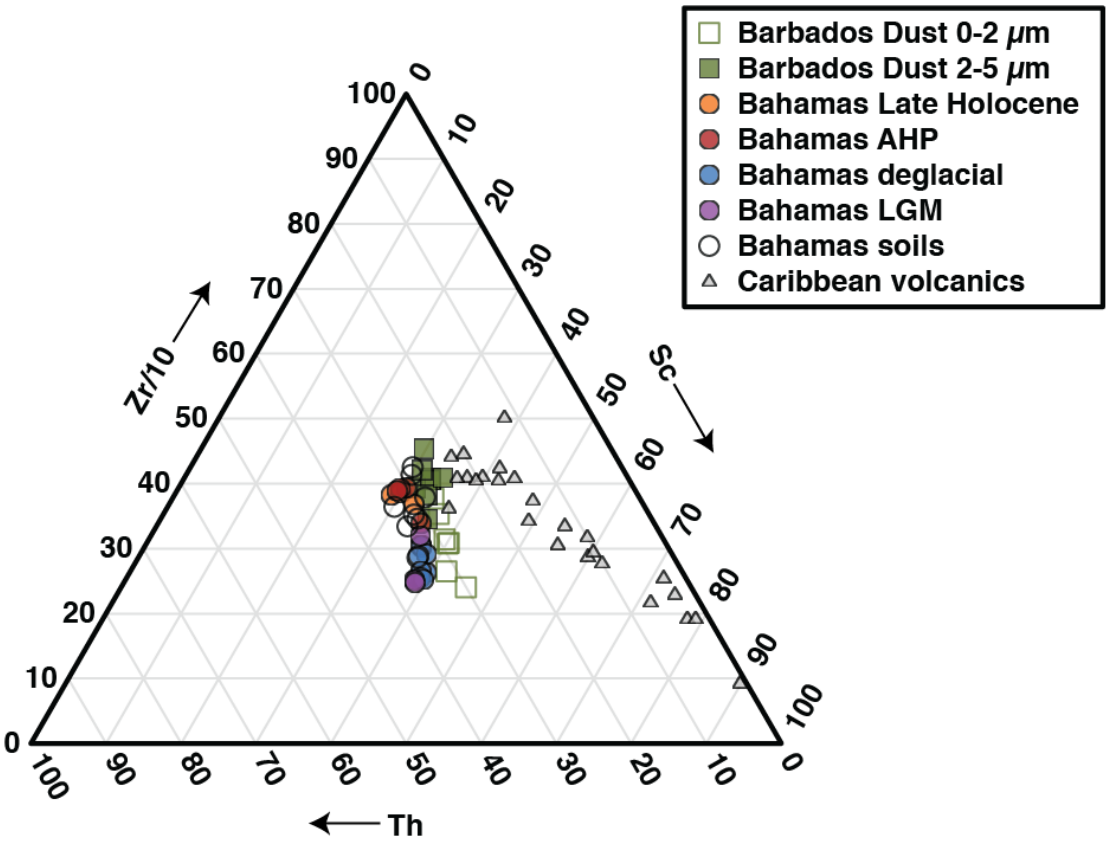

fig. S7. Ternary diagram comparing the trace element compositions of Bahamas sediments and soils and potential sources of terrigenous sediment. The data show substantial agreement between Bahamas sediments, Bahamas soils and African dust collected in Barbados, consistent with African dust being the primary source of terrigenous material in these sediments. LGM and deglacial sediments in the Bahamas have a slightly different composition from Holocene sediments, perhaps due to a slight change of dust provenance or grain size. Zr concentrations have been divided by 10. Data for African dust, Bahamas soils and Caribbean soils are from (*11*).

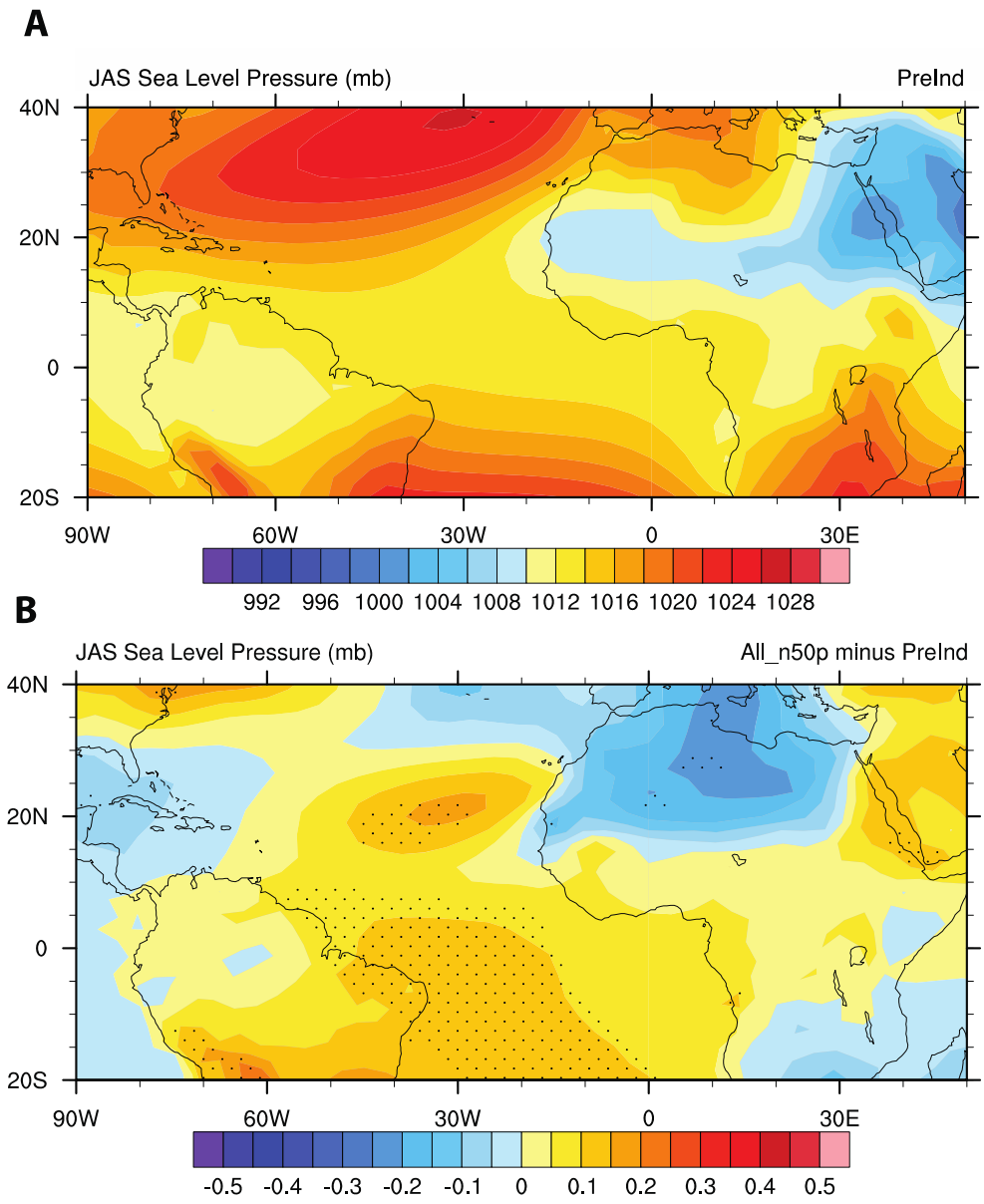

fig. S8. Sea-level pressure changes in the GCM experiment. (**A**) Sea-level pressure in JAS in the preindustrial control experiment. (**B**) Sea-level pressure anomalies in the perturbed low-dust experiment ("All_n50p") relative to the control. Note the strong low-pressure anomaly over the northern Sahara and the meridional surface pressure gradient over the continent, driving anomalous southwesterly moisture transport into the Sahel and southern Sahara in response to reduced dust loading over the TNA.

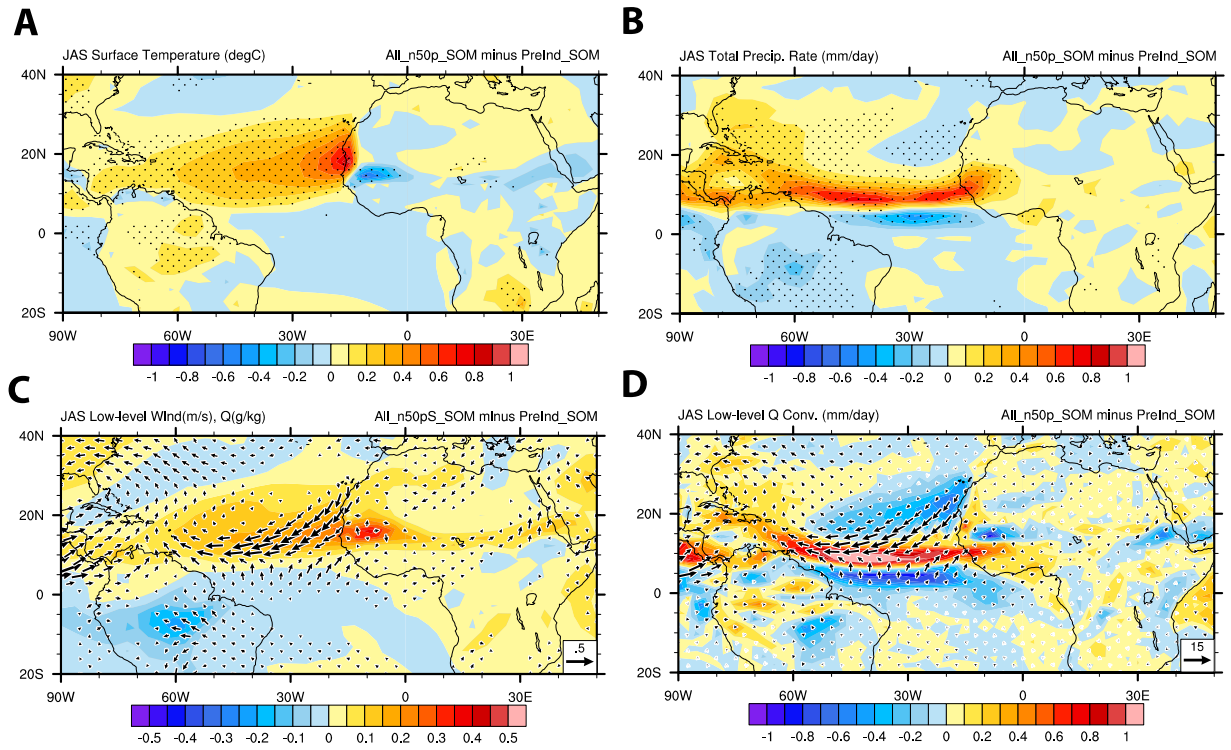

fig. S9. Slab ocean simulation of the impacts of reduced dust loading over the subtropical North Atlantic. Panels show JAS changes in the reduced dust simulation ("All_n50p_SOM") relative to the preindustrial control for (**A**) surface temperature in ˚C; (**B**) precipitation in mm/day; (**C**) low-level specific humidity (g/kg) and winds (vectors; m/s); (**D**) low-level water vapor convergence (mm/day) and water vapor transport (vectors; kg*m/s). Low-level is defined as an average from the surface to approximately 830 hPa. Stippling in panels A and B indicates significance at p<0.1. "SOM" stands for "slab-ocean model". Note the similar spatial structure in panel B and that in fig. S11B.

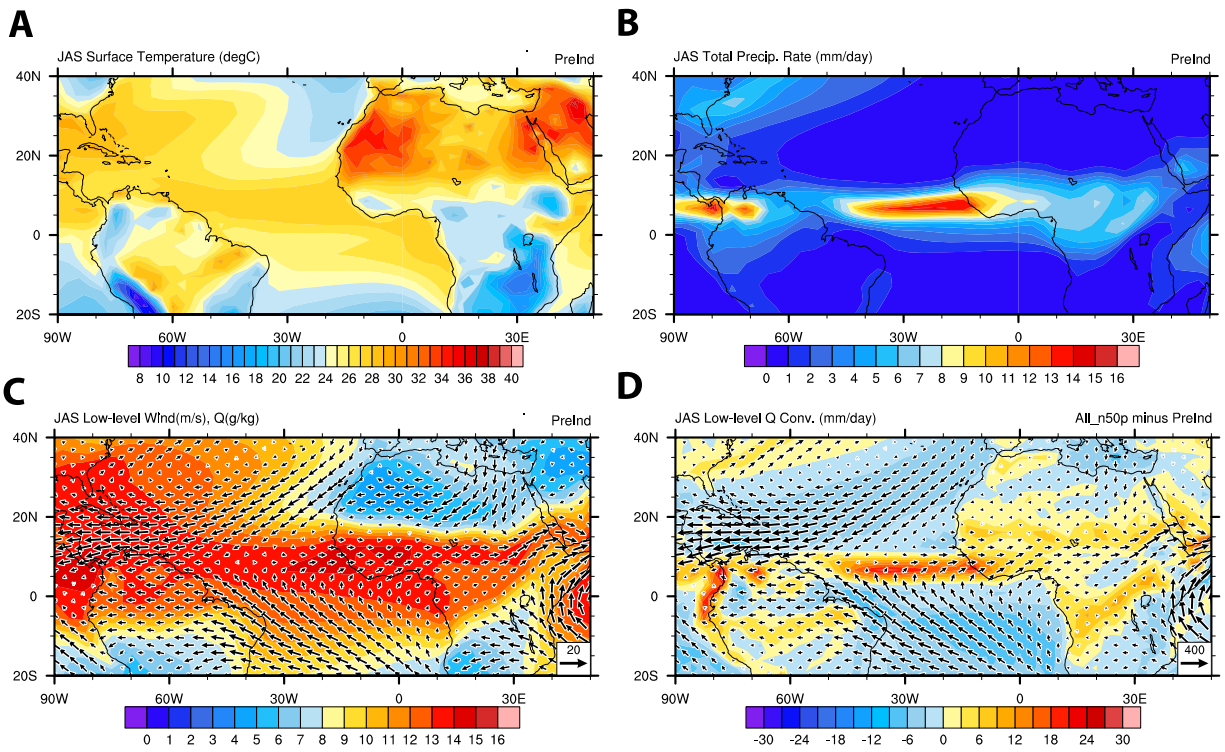

fig. S10. Climate mean state from the preindustrial control run of the coupled climate model. Panels show JAS results for (**A**) surface temperature in ˚C; (**B**) precipitation in mm/day; (**C**) low-level specific humidity (g/kg) and winds (vectors; m/s); (**D**) low-level water vapor convergence (mm/day) and water vapor transport (vectors; kg*m/s). Low-level is defined as an average from the surface to approximately 830 hPa.

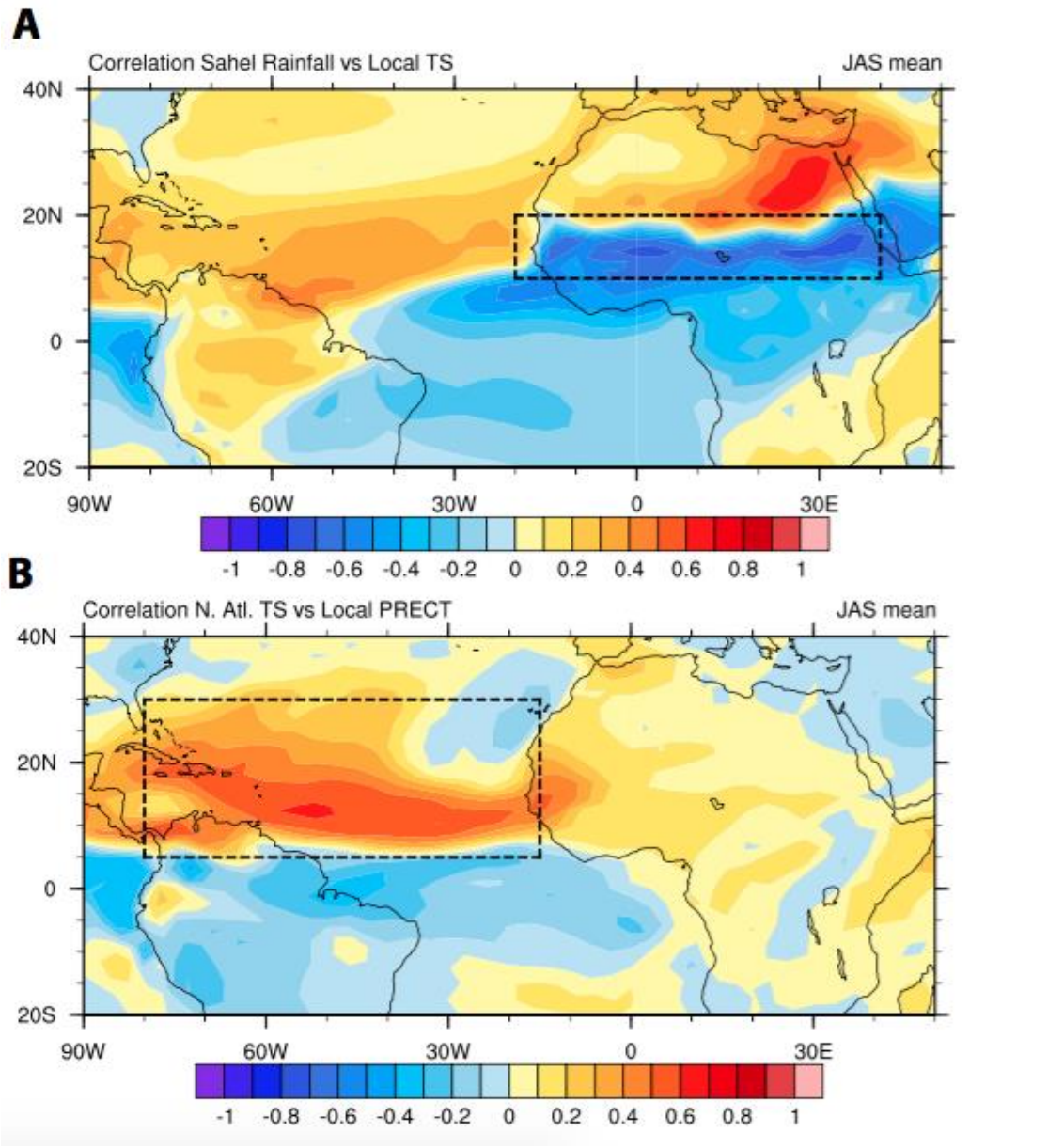

fig. S11. Relationship between surface temperatures and rainfall in the preindustrial slab ocean control simulation. (**A**) A correlation map between summer (JAS) Sahel precipitation (averaged within the black dashed box) and local surface temperature. (**B**) A correlation map between summer (JAS) TNA surface temperature (averaged within the black dashed box) and local precipitation. Both panels confirm the importance of TNA SST for Sahel rainfall, particularly in the western portion of the continent. The similarity of panel B to the precipitation response to reduced dust loading shown in Fig. 3B suggests that SST changes drive the precipitation response.

Data files:

data file S1. U-Th data and dust fluxes.

data file S2. Radiocarbon data from core VM20-234.

data file S3. Trace element data from Bahamas sediments.